Design Optimization of a Cartesian Parallel Manipulator

Han Sung Kim

Lung-Wen Tsai
e-mail: hkim@engr.ucr.edu

Department of Mechanical Engineering,
Bourns College of Engineering,
University of California,
Riverside, CA 92521

This paper introduces a 3-DOF translational parallel manipulator called Cartesian Parallel Manipulator (CPM). The manipulator consists of a moving platform that is connected to a fixed base by three limbs. Each limb is made up of one prismatic and three revolute joints and all joint axes are parallel to one another. In this way, each limb provides two rotational constraints to the moving platform and the combined effects of the three limbs lead to an over-constrained mechanism with three translational degrees of freedom. The manipulator behaves like a conventional X-Y-Z Cartesian machine due to the orthogonal arrangement of the three limbs. Two actuation methods are analyzed. However, the rotary actuation method is discarded because of the existence of singularities within the workspace. For the linear actuation method, there exists a one-to-one correspondence between the input and output displacements of the manipulator. The effects of misalignment of linear actuators on the motion of the moving platform are discussed. Each limb structure is exposed to a bending moment induced by external forces exerted on the moving platform. In order to minimize the deflection at the joints caused by the bending moment, a method to maximize the stiffness is suggested. A numerical example of the optimal design is presented. [DOI: 10.1115/1.1543977]

1 Introduction

Parallel manipulators have been studied extensively for applications that require high speed, accuracy, and stiffness. Among various types of parallel manipulators, the Gough-Stewart platform has attracted most attention because it has six degrees of freedom (DOF) and all the linear actuators are under pure forces. However, the manipulator has some disadvantages such as complex forward kinematics, small workspace, and complicated universal and spherical joints.

To overcome the above shortcomings, parallel manipulators with fewer than six degrees of freedom have been investigated. A manipulator with fewer than six degrees of freedom costs less than a 6-DOF counterpart and, hence, it may be more economic to employ such manipulators for applications for which 6-DOF is not necessary. For examples, Lee and Shah [1] analyzed a 3-DOF parallel manipulator with three *RPS* (revolute-prismatic-spherical) chains. Yang et al. [2] developed a low-cost driving simulator using the 3-*RPS* manipulator. Ceccarelli [3] proposed a 3-DOF parallel manipulator (called CaPaMan) in which each leg mechanism is made up of a planar parallelogram, a prismatic joint, and a ball joint. However, these manipulators have coupled motion between the position and orientation of the end effector. Recent research on 3-DOF parallel manipulators has been leaning toward the decoupling of the position and orientation of the end-effector and the elimination of complicated multi-DOF joints. Three-DOF parallel manipulators with a rotational or translational moving platform have been investigated. The classical 3-*RRR* spherical manipulator was studied in detail by Gosselin and Angeles [4]. Other spatial parallel manipulators with a rotational moving platform, called rotational parallel manipulators (RPMs), have been proposed [5–8]. The structural synthesis of 3-DOF RPMs has been carried out by Fang and Tsai [9]. For translational parallel manipulators (TPMs), Clavel [10] invented a simple and fast parallel manipulator called the DELTA robot, which was analyzed in more detail by Pierrot et al. [11]. Tsai et al. [12,13] designed a 3-DOF TPM that employs only revolute joints and planar parallelograms. Tsai [14] presented the design of a spatial 3-*UPU* (universal-prismatic-universal) manipulator and pointed out the conditions that lead to pure translational motion. The kinematics of the 3-*UPU* manipulator was studied further by Di Gregorio and Parenti-Castelli [15], and Tsai and Joshi [16]. Tsai and Joshi [17] analyzed the kinematics of four TPMs for use in hybrid kinematic machines. Herve and Sparcino [18] presented a comprehensive list of 4-DOF limb structures for overconstrained TPMs, including a *CRR* chain. They showed that only two *CRR* limbs are sufficient to generate 3-DOF translational motion and the third limb is just compatible with the first two. Zhao and Huang [19] studied the kinematics of an over-constrained 3-*RRC* (revolute-revolute-cylindrical) TPM. Wenger and Chablat [20] suggested the use of a 3-DOF TPM as a machine tool, called the Orthoglide. Although the three linear actuators in the Orthoglide are arranged orthogonally, its Jacobian matrix is isotropic only at the center point of the workspace. Baron and Bernier [21,22] studied the design of a 3-DOF Star manipulator conceived by Herve [23]. Carricato and Parenti-Castelli [24,25] developed a family of 3-DOF TPMs. Kong and Gosselin [26,27] performed the type synthesis of linear TPMs and found several input-output decoupled linear TPMs. Fang and Tsai [28] presented a systematic methodology for structure synthesis 3-DOF TPMs using the theory of reciprocal screws. Carricato and Parenti-Castelli [29,30][1] studied isotropic TPMs. A 3-CRR TPM similar to the CPM presented in this paper was analyzed by Kong and Gosselin [31].[1]

In this paper, a parallel manipulator that employs only revolute and prismatic joints to achieve translational motion of the moving platform is presented. In what follows, the kinematic architecture of the manipulator is described. Then two actuation methods are discussed. For the rotary actuation method, it is shown that the inverse kinematics provides two solutions per limb, and the forward kinematics leads to an eighth-degree polynomial. It is also shown that the rotary actuation method results in many singular points within the workspace. On the other hand, for the linear actuation method, there exists a one-to-one correspondence between the input and output displacements of the manipulator. Due to the orthogonal arrangement of the limbs, the Jacobian matrix is always isotropic and the manipulator behaves like a traditional X-Y-Z Cartesian machine. Hence, the control algorithm can be very simple. The effects of misalignment of linear actuators on the motion of the moving platform are discussed. Each limb structure

Contributed by the Mechanisms and Robotics Committee for publication in the JOURNAL OF MECHANICAL DESIGN. Manuscript received January 2002; Revised July 2002. Associate Editor: M. Raghavan.

[1]After this paper was accepted for publication, we became aware of these papers that are either in print or under review.

is exposed to a bending moment induced by the external force exerted on the end-effector. In order to minimize the deflection at the joints caused by the bending moment, a method to maximize the stiffness is suggested. Finally, a numerical example of the optimal design is presented.

2 Geometry of the Manipulator

The kinematic structure of the Cartesian parallel manipulator is shown in Fig. 1 where a moving platform is connected to a fixed base by three *PRRR* (prismatic-revolute-revolute-revolute) limbs. The moving platform is symbolically represented by a circle defined by B_1, B_2, and B_3 and the fixed base is defined by three guide rods passing through A_1, A_2, and A_3, respectively. The three revolute joint axes in each limb are located at points A_i, M_i, and B_i, respectively, and are parallel to the ground-connected prismatic joint axis. Furthermore, the three prismatic joint axes, passing through point A_i for $i=1$, 2, and 3, are parallel to the X, Y, and Z axes, respectively. Specifically, the first prismatic joint axis lies on the X axis; the second prismatic joint axis is parallel to the Y axis with an offset e_z in the Z direction; and the third prismatic joint axis is parallel to the Z axis with an offset e_x in the X direction and e_y in the Y direction. Point P represents the center of the moving platform. The link lengths are denoted by l_{i1}, l_{i2}, and l_3, respectively. The starting point of a prismatic joint is defined by d_{0i} and the sliding distance is defined by d_i. Note that each *PRRR* limb is equivalent to a *CRR* limb. In this regard, the 3-*PRRR* parallel manipulator is a kinematic inversion of the 3-*RRC* manipulator. Also note that the third prismatic joint axis is purposely located far away from the Z-axis to avoid mechanical interference among the three limbs.

For simplicity, three local coordinate systems are introduced with their origins located at A_i. The Z_1, Z_2, and Z_3 axes are parallel to the X, Y, and Z axes, and the X_1, X_2, and X_3 axes are parallel to the Y, Z, and X axes, respectively, as shown in Fig. 1.

Due to the three parallel revolute joints located at points A_i, M_i, and B_i, any single limb constrains the moving platform from rotating about the local X_i and Y_i axes. Since each limb provides two rotational constraints to the moving platform, the combined effects result in three redundant constraints on the rotation of the moving platform and, therefore, completely constrain the moving platform from rotation. This leaves the moving platform with three translational degrees of freedom.

Figure 2 shows the joint angles of a limb with respect to the local coordinate system. We note that the joint angles of links $\overline{A_iM_i}$, $\overline{M_iB_i}$, and $\overline{B_iP}$ with respect to the local X axis are denoted by θ_{i1}, θ_{i2}, and θ_{i3}, respectively. The angle between $\overline{A_iB_i}$ and the X_i axis is denoted by θ_{ia}, the angle between lines $\overline{A_iM_i}$ and $\overline{A_iB_i}$ is denoted by θ_{ib}, and the angle between the extended line of $\overline{A_iM_i}$ and $\overline{M_iB_i}$ is denoted by θ_{i2}^*. Further, ${}^i\mathbf{r}_{ij}$ denotes a common perpendicular vector between the two revolute joint axes of a link, where the first subscript denotes the limb number, the second subscript represents the link number of a limb, and the leading superscript is used to denote the coordinate system with respect to which a vector is expressed.

Figure 3 shows two methods of actuation, namely, linear and rotary actuation methods. In the following, we discuss the kinematics of each actuation method in turn.

3 Rotary Actuation Method

For the rotary actuation method, a rotary actuator drives the first revolute joint of each limb whereas all the other joints are passive.

3.1 Inverse Kinematics. The inverse kinematics is to find

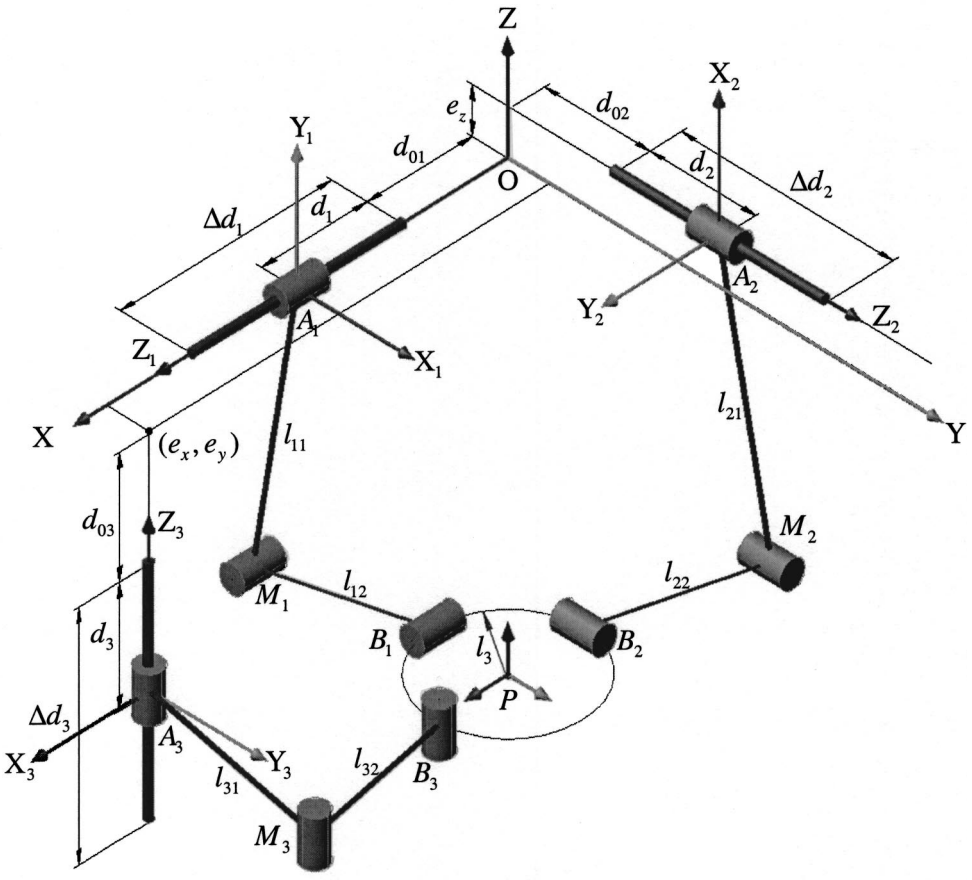

Fig. 1 Spatial 3-*PRRR* parallel manipulator

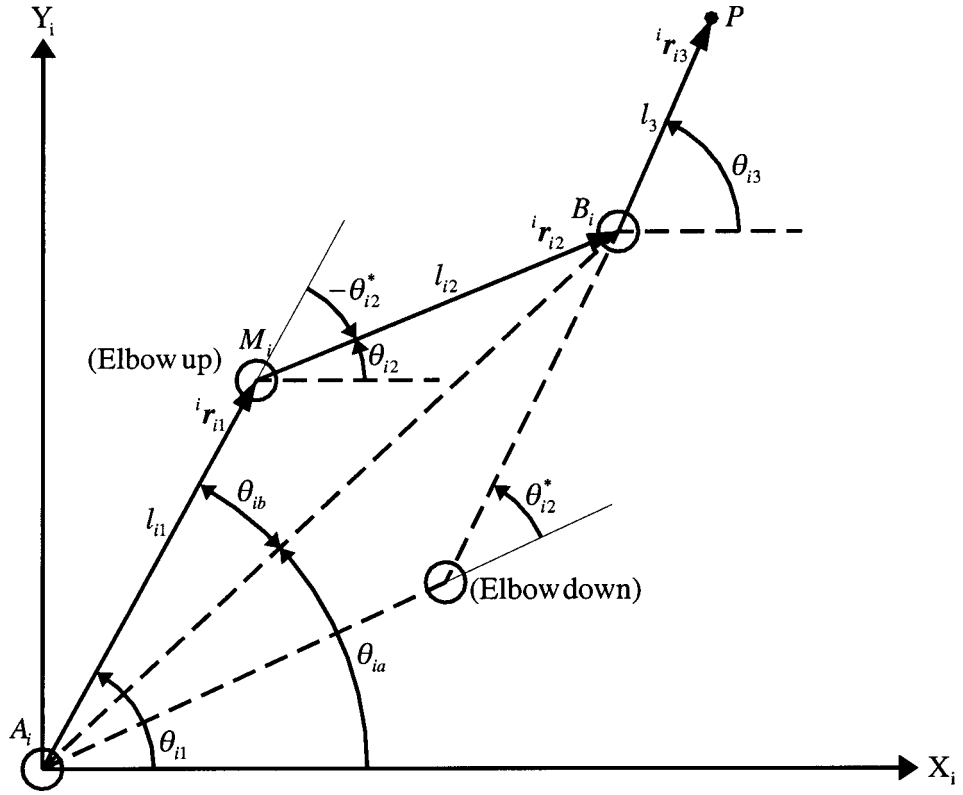

Fig. 2 Joint angles of the *i*th limb with respect to the *i*th limb coordinate system

the input joint angles, θ_{i1}, for $i=1$, 2, and 3, for a given end-effector position, $\mathbf{p}=[p_x, p_y, p_z]^T$. From the geometry given in Fig. 1, we obtain the position vectors of B_i with respect to each local coordinate system as follows:

$$ {}^1\mathbf{B}_1=\begin{bmatrix} p_y-l_3 \\ p_z \\ 0 \end{bmatrix}, \quad {}^2\mathbf{B}_2=\begin{bmatrix} p_z-e_z \\ p_x-l_3 \\ 0 \end{bmatrix}, \quad \text{and} $$

$$ {}^3\mathbf{B}_3=\begin{bmatrix} p_x+l_3-e_x \\ p_y-e_y \\ 0 \end{bmatrix}. \tag{1} $$

Referring to Fig. 2, the input joint angles, θ_{i1}, are found as follows:

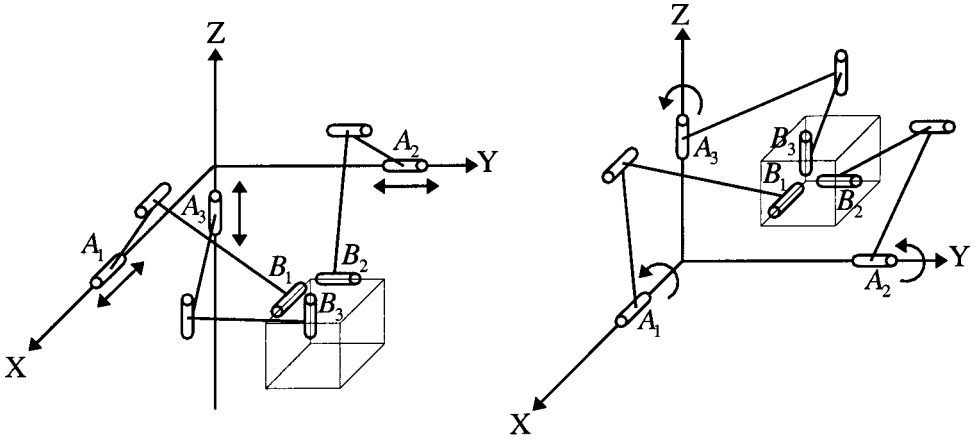

(*a*) Linear actuation method (*b*) Rotary actuation method

Fig. 3 Linear and rotary actuation methods

$$\theta_{i1}=\theta_{ia}\pm\theta_{ib}=\tan^{-1}\frac{{}^iB_{iy}}{{}^iB_{ix}}\pm\cos^{-1}\frac{l_{i1}^2+{}^iB_{ix}^2+{}^iB_{iy}^2-l_{i2}^2}{2l_{i1}\sqrt{{}^iB_{ix}^2+{}^iB_{iy}^2}},$$

$$\text{for}\quad i=1,\ 2,\ \text{and}\ 3. \tag{2}$$

Due to finite reach of each limb, the following constraint, which represents the minimum and maximum reaches of a serial chain, must be satisfied:

$$(l_{i1}-l_{i2})^2\leqslant{}^iB_{ix}^2+{}^iB_{iy}^2\leqslant(l_{i1}+l_{i2})^2. \tag{3}$$

3.2 Forward Kinematics. The forward kinematics is to obtain the end-effector position, $[p_x,p_y,p_z]^T$, when the input joint angles, θ_{i1} for $i=1$, 2, and 3, are given.

Referring to Fig. 2, the second link length can be written in terms of the locations of the second and third revolute joints as follows:

$$({}^iB_{ix}-l_{i1}C\theta_{i1})^2+({}^iB_{iy}-l_{i1}S\theta_{i1})^2=l_{i2}^2, \tag{4}$$

where $C\theta_{i1}=\cos\theta_{i1}$ and $S\theta_{i1}=\sin\theta_{i1}$. Substituting Eq. (1) into (4) yields

$$\begin{aligned}&[p_y-(l_{11}C\theta_{11}+l_3)]^2+[p_z-l_{11}S\theta_{11}]^2=l_{12}^2,\\ &[p_z-(l_{21}C\theta_{21}+e_z)]^2+[p_x-(l_{21}S\theta_{21}+l_3)]^2=l_{22}^2,\\ &[p_x-(l_{31}C\theta_{31}+e_x-l_3)]^2+[p_y-(l_{31}S\theta_{31}+e_y)]^2=l_{32}^2.\end{aligned} \tag{5}$$

Eliminating p_y and p_z from Eq. (5) gives an eighth-degree polynomial in p_x:

$$c_8p_x^8+c_7p_x^7+c_6p_x^6+c_5p_x^5+c_4p_x^4+c_3p_x^3+c_2p_x^2+c_1p_x+c_0=0. \tag{6}$$

Hence, at most eight different manipulator configurations are possible for the forward kinematics.

3.3 Jacobian, Singularity, and Static Force Analyses. Differentiating Eq. (1) with respect to time yields the velocities of B_i, for $i=1$, 2, and 3, relative to and expressed in their respective local coordinate systems as follows:

$${}^1\dot{\mathbf{B}}_1=\begin{bmatrix}\dot p_y\\ \dot p_z\\ 0\end{bmatrix},\quad {}^2\dot{\mathbf{B}}_2=\begin{bmatrix}\dot p_z\\ \dot p_x\\ 0\end{bmatrix},\quad \text{and}\quad {}^3\dot{\mathbf{B}}_3=\begin{bmatrix}\dot p_x\\ \dot p_y\\ 0\end{bmatrix}. \tag{7}$$

Referring to Fig. 2, the linear velocity of B_i relative to the local coordinate system can be written in terms of the joint rates as

$$\begin{aligned}{}^i\dot B_{ix}&=-\dot\theta_{i1}l_{i1}S\theta_{i1}-\dot\theta_{i2}l_{i2}S\theta_{i2},\\ {}^i\dot B_{iy}&=\dot\theta_{i1}l_{i1}C\theta_{i1}+\dot\theta_{i2}l_{i2}C\theta_{i2}.\end{aligned} \tag{8}$$

Eliminating $\dot\theta_{i2}$ in Eq. (8) yields

$${}^i\dot B_{ix}C\theta_{i2}+{}^i\dot B_{iy}S\theta_{i2}=l_{i1}S(\theta_{i2}-\theta_{i1})\dot\theta_{i1}. \tag{9}$$

Substituting Eq. (7) into (9), we obtain an input-output velocity relationship as follows:

$$J_x\dot{\mathbf{p}}=J_q\dot{\boldsymbol\theta}_1 \tag{10}$$

where

$$\dot{\mathbf{p}}=[\dot p_x,\dot p_y,\dot p_z]^T,$$

$$\dot{\boldsymbol\theta}_1=[\dot\theta_{11},\dot\theta_{21},\dot\theta_{31}]^T,$$

$$J_x=\begin{bmatrix}0 & C\theta_{12} & S\theta_{12}\\ S\theta_{22} & 0 & C\theta_{22}\\ C\theta_{32} & S\theta_{32} & 0\end{bmatrix},$$

$$J_q=\begin{bmatrix}l_{11}S(\theta_{12}-\theta_{11}) & 0 & 0\\ 0 & l_{21}S(\theta_{22}-\theta_{21}) & 0\\ 0 & 0 & l_{31}S(\theta_{32}-\theta_{31})\end{bmatrix}.$$

Hence, if $S(\theta_{i2}-\theta_{i1})\neq0$, the inverse velocity transformation can be written as

$$\dot{\boldsymbol\theta}_1=J\dot{\mathbf{p}} \tag{11}$$

where

$$J\equiv J_q^{-1}J_x \tag{12}$$

is called the *Jacobian matrix* of the manipulator.

Next, singular configurations of the manipulator are examined. If $\det(J_q)=0$, the joint rates cannot be determined. Hence, an inverse kinematic singularity [32] occurs when the first and second links of any limb are collinear; that is, when

$$S(\theta_{i2}-\theta_{i1})=0. \tag{13}$$

A direct kinematic singularity [32] occurs when $\det(J_x)=0$ or equivalently

$$C\theta_{12}C\theta_{22}C\theta_{32}+S\theta_{12}S\theta_{22}S\theta_{32}=0. \tag{14}$$

Since Eq. (14) is satisfied for any combination of $C\theta_{i2}=0$ and $S\theta_{j2}=0$ for $i\neq j$, we conclude that there exist many direct kinematic singularities. For example, when the manipulator assumes a configuration of $\theta_{12}=0°$, $\theta_{22}=90°$, and $\theta_{32}=$any, it becomes singular. Since such singularity may occur within the workspace, the rotary actuation method is judged to be impractical.

For static force analysis, it is assumed that link weights and joint friction are negligible. Applying the principle of virtual work, a static force relation is obtained:

$$\mathbf{f}=J^T\boldsymbol\tau \tag{15}$$

where $\mathbf{f}=[f_x,f_y,f_z]^T$ denotes a vector of end-effector output forces and $\boldsymbol\tau=[\tau_{11},\tau_{21},\tau_{31}]^T$ represents a vector of actuator input torques.

4 Linear Actuation Method

For the linear actuation method, a linear actuator drives the prismatic joint in each limb whereas all the other joints are passive. This method has the advantage of having all actuators installed on the fixed base.

4.1 Forward and Inverse Kinematics. The forward and inverse kinematic analyses are trivial since there exists a one-to-one correspondence between the end-effector position and the input joint displacements. Referring to Fig. 1, each limb constrains point P to lie on a plane which passes through point A_i and is perpendicular to the axis of the linear actuator. Consequently, the location of P is determined by the intersection of three planes. A simple kinematic relation can be written as

$$\begin{bmatrix}p_x\\ p_y\\ p_z\end{bmatrix}=\begin{bmatrix}d_{01}+d_1\\ d_{02}+d_2\\ d_{03}+d_3\end{bmatrix}. \tag{16}$$

4.2 Jacobian and Static Force Analyses. The velocity and output force of the end-effector also have a one-to-one relationship with that of the linear actuators. Taking the derivative of Eq. (16) with respect to time yields

$$\begin{bmatrix}\dot d_1\\ \dot d_2\\ \dot d_3\end{bmatrix}=J\begin{bmatrix}\dot p_x\\ \dot p_y\\ \dot p_z\end{bmatrix} \tag{17}$$

where J is the 3×3 identity matrix. Since J is an identity matrix, the manipulator is isotropic everywhere within its workspace.

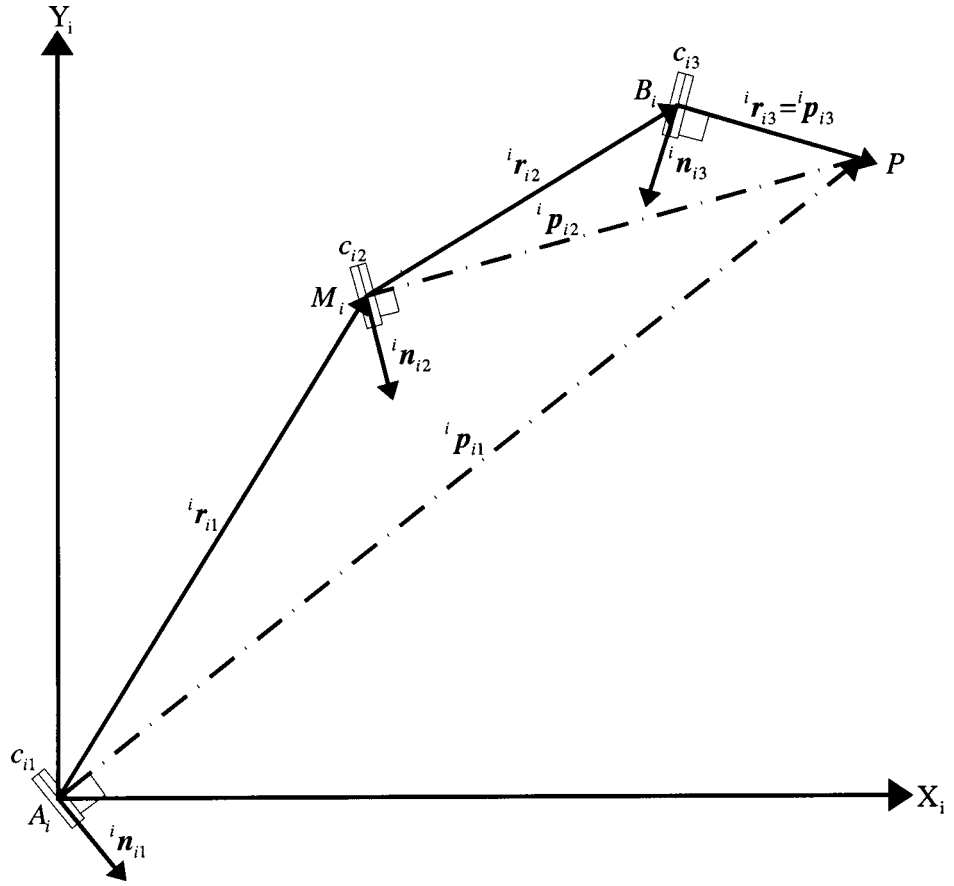

Fig. 4 A serial manipulator made up of three compliant joints

Neglecting gravitational forces of the links and frictional forces in the joints and applying the principle of virtual work, we obtain

$$\begin{bmatrix} f_x \\ f_y \\ f_z \end{bmatrix} = J^T \begin{bmatrix} f_1 \\ f_2 \\ f_3 \end{bmatrix} \tag{18}$$

where $[f_x, f_y, f_z]^T$ denotes a vector of end-effector output forces and $[f_1, f_2, f_3]^T$ denotes a vector of linear actuator forces. We observe that due to the orthogonal arrangement of the linear actuators, there exists a one-to-one correspondence between the vector of actuator input forces and that of the end-effector output forces.

Because of the de-coupled X, Y, and Z motions and the isotropic characteristics of the Jacobian matrix, the linear actuation method is chosen for further analysis and prototype development.

4.3 Stiffness Modeling. Figure 4 shows the ith limb sketched in its local coordinate system where the revolute joint axes at points A_i, M_i, and B_i (not shown) are all perpendicular to the $X_i - Y_i$ plane, ${}^i\mathbf{r}_{ij}$ denotes the common perpendicular vector between the two revolute joint axes of the jth link, and ${}^i\mathbf{p}_{ij}$ denotes a vector pointing from the jth revolute joint to point P in the moving platform. Following the above definitions, we have ${}^i\mathbf{p}_{i1} = {}^i\mathbf{r}_{i1} + {}^i\mathbf{r}_{i2} + {}^i\mathbf{r}_{i3}$, ${}^i\mathbf{p}_{i2} = {}^i\mathbf{r}_{i2} + {}^i\mathbf{r}_{i3}$, and ${}^i\mathbf{p}_{i3} = {}^i\mathbf{r}_{i3}$.

We note that, excluding the prismatic joint, each limb form a planar 3-DOF open-loop chain. Since the revolute joints in each limb are free to rotate, linear actuator force can only be transmitted in a direction parallel to the revolute joint axes; that is, along the local Z_i axis. When this force is resisted by the external force exerted on the moving platform, it generates a bending moment ${}^i\mathbf{n}_{ij}$ in each joint about an axis perpendicular to both vectors ${}^i\mathbf{p}_{ij}$ and Z_i as shown in Fig. 4. Assume that all links are rigid and the major source of compliance comes from the flexibility of the bearings in the joints. Then, the deflection between two members of a revolute joint can be modeled as an infinitesimal rotation about the axis of the bending moment. We call such an axis of deflection a ''virtual axis'' of compliance. The virtual axis of compliance coincides with the direction of the bending moment. Hence, we may consider each limb together with the moving platform as a serial manipulator having three virtual axes of compliance.

Referring to Fig. 2, the vector ${}^k\mathbf{r}_{ij}$ of each link can be expressed in the local coordinate system as follows:

$${}^i\mathbf{r}_{i1} = l_{i1}\begin{bmatrix} C\theta_{i1} \\ S\theta_{i1} \\ 0 \end{bmatrix}, \quad {}^i\mathbf{r}_{i2} = l_{i2}\begin{bmatrix} C\theta_{i2} \\ S\theta_{i2} \\ 0 \end{bmatrix}, \quad \text{and} \quad {}^i\mathbf{r}_{i3} = l_{i3}\begin{bmatrix} C\theta_{i3} \\ S\theta_{i3} \\ 0 \end{bmatrix} \tag{19}$$

Following the definition of a local coordinate system, we have $\theta_{13} = 0$, $\theta_{23} = \pi/2$ and $\theta_{33} = \pi$ (see Fig. 1).

As shown in Fig. 4, let ${}^i\mathbf{n}_{ij}$ be the reaction moment exerted on link j by link $j-1$ of the ith limb, and ${}^i\mathbf{f}_i = [0,0,f_{iz}]^T$ be the force exerted on the moving platform by the ith limb. A simple moment balance analysis yields

$${}^i\mathbf{n}_{ij} = {}^i\mathbf{p}_{ij} \times {}^i\mathbf{f}_i \,. \tag{20}$$

A small angular deflection of one link with respect to the other about the virtual axis of compliance, $\delta\theta_{ij}$, can be modeled as

$${}^i\delta\theta_{ij} = c_{ij} n_{ij} \tag{21}$$

where c_{ij} is the angular compliance constant associated with the bearings of the jth joint of the ith limb, $p_{ij} = \|{}^i\mathbf{p}_{ij}\|$, and $n_{ij} = \|{}^i\mathbf{n}_{ij}\| = p_{ij} f_{iz}$ since ${}^i\mathbf{p}_{ij}$ and ${}^i\mathbf{f}_i$, are perpendicular.

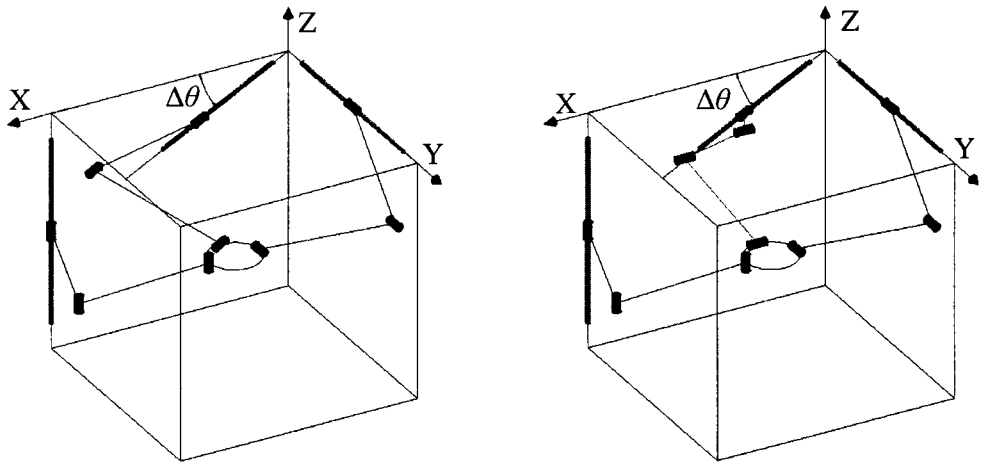

(*a*) Misaligned X drive (*b*) Misaligned X drive with compensation

Fig. 5 Manipulator with a misaligned X actuator

Since the displacement of the moving platform caused by an infinitesimal rotation of $\delta\theta_{ij}$ about the jth joint axis of the ith limb is equal to $\delta\theta_{ij}p_{ij}$ and it is parallel to the Z_i axis, the total displacement of the moving platform, caused by infinitesimal rotations about the three revolute joints, is given by

$$(c_{i1}p_{i1}^2+c_{i2}p_{i2}^2+c_{i3}p_{i3}^2)f_{iz}. \tag{22}$$

From Eq. (18), it can be concluded that the X-component of the end-effector output force will only deflect the X-limb in the X-direction and so on. Hence, the overall deflection at the moving platform is simply a summation of the deflections of the three limbs. Equation (22) written three times, once for each limb, $i=1$, 2, and 3, yields

$$\begin{aligned}\delta p_x&=(c_{11}p_{11}^2+c_{12}p_{12}^2+c_{13}p_{13}^2)f_x\\ \delta p_y&=(c_{21}p_{21}^2+c_{22}p_{22}^2+c_{23}p_{23}^2)f_y\\ \delta p_z&=(c_{31}p_{31}^2+c_{32}p_{32}^2+c_{33}p_{33}^2)f_z\end{aligned} \tag{23}$$

Writing Eq. (23) in matrix form, we obtain

$$\delta\mathbf{p}=C\mathbf{f} \tag{24}$$

where $\delta\mathbf{p}=[\delta p_x,\delta p_y,\delta p_z]^T$ and $\mathbf{f}=[f_x,f_y,f_z]^T$. The matrix C, called the *compliance matrix*, is a 3×3 diagonal matrix whose diagonal elements are given by

$$C_{ii}=c_{i1}p_{i1}^2+c_{i2}p_{i2}^2+c_{i3}p_{i3}^2. \tag{25}$$

Multiplying Eq. (25) by C^{-1}, we obtain

$$\mathbf{f}=K\delta\mathbf{x} \tag{26}$$

where $K=C^{-1}$ is called the *stiffness matrix* of the manipulator.

4.4 Tolerance Consideration. In practice, it may be difficult to fabricate and assemble a perfectly orthogonal frame. In this section, we illustrate a method for compensating the manufacturing and assembling errors of the linear actuators by an example. We assume that the X actuator is skewed by a small angle $\Delta\theta$ about the global Z-axis, and the other actuators are mounted perfectly along the Y and Z axes, respectively, as shown in Fig. 5.

First, we assume that the revolute joint axes in the X limb remain parallel to each other and to the prismatic joint axis as shown in Fig. 5(*a*). Figure 6(*a*) shows that with the X and Z actuators held stationary, the locus of B_2 follows the dotted line as

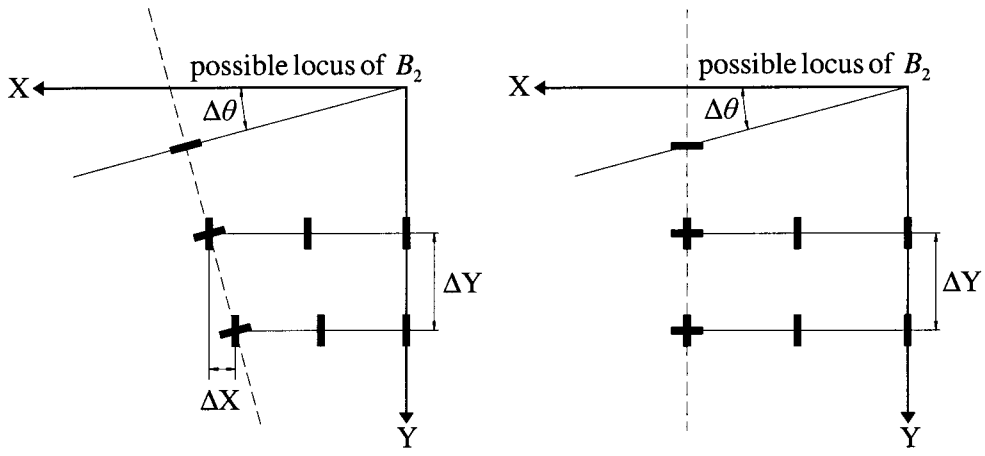

(*a*) Misaligned X drive (*b*) Misaligned X drive with compensation

Fig. 6 Top view of a misaligned actuator

the Y-actuator moves along the Y-axis. Therefore, it can be concluded that if the revolute joint axes of the X limb remain parallel to the prismatic joint, the x, y, and z motions of the moving platform become slightly coupled.

The coupling problem can be solved by adjusting the orientation of the X limb such that the revolute joint axes are parallel to the global X-axis instead of the prismatic joint axis as shown in Fig. 5(*b*). In this case, the x, y, and z motions of the moving platform remain uncoupled as depicted in Fig. 6(*b*).

It should be noted that the three revolute joint axes in each limb must be always parallel to one another. Otherwise, the manipulator may not move or the motion may depend on the deflection of the links.

5 Design Optimization

The design optimization given below makes an attempt to maximize the stiffness of the manipulator for a given workspace volume. To optimize the design, the average stiffness constant in the sense of Euclidean norm is considered,

$$k_{\text{ave}} \equiv \sqrt{k_{11}^2 + k_{22}^2 + k_{33}^2} \tag{27}$$

where k_{ii} for $i=1$, 2, and 3 denote the diagonal elements of the stiffness matrix K. We assume that $c_{ij}=c$ for all joints. It follows from Eq. (25) that the average stiffness constant can be factored into the product of a constant term and a geometric term,

$$k_{\text{ave}} = \frac{1}{c}\sqrt{\frac{1}{\left(\sum_{j=1}^{3} p_{1j}^2\right)^2} + \frac{1}{\left(\sum_{j=1}^{3} p_{2j}^2\right)^2} + \frac{1}{\left(\sum_{j=1}^{3} p_{3j}^2\right)^2}}. \tag{28}$$

Multiplying both side of Eq. (28) by c eliminates the constant term. Hence, a local design index (LDI) is defined as

$$\text{LDI} \equiv c k_{\text{ave}} = \sqrt{\frac{1}{\left(\sum_{j=1}^{3} p_{1j}^2\right)^2} + \frac{1}{\left(\sum_{j=1}^{3} p_{2j}^2\right)^2} + \frac{1}{\left(\sum_{j=1}^{3} p_{3j}^2\right)^2}}. \tag{29}$$

The workspace of the manipulator may be limited by the link lengths and angular rotation limits of the revolute joints, or by the stroke lengths of the linear actuators. However, it is preferable to make the limb lengths sufficiently long such that the ranges of motion of all linear actuators can be fully utilized. To achieve this goal, we impose the constraint that the workspace volume is always equal to the product of the stroke lengths of the linear actuators. Hence, the optimal design problem is formulated as

$$\text{Maximize:} \quad \eta = \frac{1}{W}\int_W \text{LDI}\, dW$$

$$\text{Subject to:} \quad W = \Delta d_1 \times \Delta d_2 \times \Delta d_3 \tag{30}$$

where W and dW denote the total workspace volume and a differential workspace, respectively, and Δd_i represents stroke length of the ith linear actuator. We call η the global design index. Dividing the global design index, η, by the angular compliance constant, c, gives a linear stiffness. Hence, the global design index can be interpreted as an average stiffness in the workspace. Since the stroke lengths are determined by a desired workspace volume, they are treated as constant parameters during the optimization process. Therefore, referring to Fig. 1, the design variables of the optimization problem are

$$[d_{0i}, l_{i1}, l_{i2}, l_3, e_x, e_y, e_z], \qquad \text{for} \quad i=1, 2, \text{and } 3. \tag{31}$$

In view of the difficulty in obtaining a closed-form solution to Eq. (30), the Monte Carlo method [33] is employed for the optimization. Specifically, given a set of design parameters, the following procedure is used for the computation of the global design index.

- Given the stroke lengths of the linear actuators, define a rectangular box with a total volume of $W=\Delta d_1 \times \Delta d_2 \times \Delta d_3$.
- Divide the box into a set of orthogonal grids and calculate the total number of grid points as n_{total}. Initialize the number of points, $n_{\text{workspace}}$, that fall within the workspace of the manipulator to zero.
- For every grid point, two conditions are evaluated to check if it falls within the workspace of the manipulator:

$$(l_{i1}-l_{i2})^2 \leqslant {}^iB_{ix}^2 + {}^iB_{iy}^2 \leqslant (l_{i1}+l_{i2})^2,$$
$$\theta_L \leqslant |\theta_{i2}^*| \leqslant \theta_H. \tag{32}$$

The first constraint comes from the minimum and maximum reaches of a 2-link serial chain. The second constraint is introduced to keep the serial chain away from the fully stretched-out, $\theta_{i2}^*=0$, and folded-back, $\theta_{i2}^*=\pm\pi$, configurations. See Fig. 2 for the definition of θ_{i2}^*. The upper and lower joint limits of θ_{i2}^* are generally chosen such that $\pi-\theta_H=\theta_L \geqslant \theta_{\text{margin}}$ (say 15°). Note that if margin angle, θ_{margin}, is too large, the workspace may be limited by the minimum and maximum reaches of the serial chains.

- If the point satisfies the above two conditions, increment $n_{\text{workspace}}$ by one and calculate the LDI by using Eq. (29).
- Repeat the above process for every grid point until all the points are accounted for and sum up the LDI for all points that fall within the workspace, $S=\Sigma\text{LDI}$.
- If $n_{\text{workspace}}$ is less than n_{total}, the set of design parameters is judged to be infeasible, since the equality constraint imposed by Eq. (30) is violated.
- If $n_{\text{workspace}}=n_{\text{total}}$, compute the global design index as:

$$\eta = \frac{S}{n_{\text{workspace}}}. \tag{33}$$

Note that when link lengths are too long, $|\theta_{i2}^*|$ may exceed the upper limit θ_H in a region around the origin. On the other hand, when the link lengths are too short, $|\theta_{i2}^*|$ may drop below the lower limit θ_L in a region far away from the origin.

6 Prototype Design

In this section, we optimize the design of a prototype manipulator. In this design, the stroke lengths of the linear actuators are chosen as follows:

$$\Delta d_1 = \Delta d_2 = 400 \quad \text{and} \quad \Delta d_3 = 300 \ (mm).$$

To make the X and Y limbs symmetrical, we assume that

$$d_{0p} \equiv d_{01} = d_{02}, \quad d_{0z} \equiv d_{03}, \quad e_z = 0,$$
$$l_{p1} \equiv l_{11} = l_{21}, \quad l_{z1} \equiv l_{31}, \quad l_{p2} \equiv l_{12} = l_{22}, \quad l_{z2} \equiv l_{32}. \tag{34}$$

Therefore, we are left with the following design variables:

$$[d_{0p}, d_{0z}, e_x, e_y, l_{p1}, l_{p2}, l_{z1}, l_{z2}, l_3]. \tag{35}$$

The lower and upper joint angle limits are set at

$$\theta_L = 30° \quad \text{and} \quad \theta_H = 150°.$$

To avoid mechanical interference, the following inequality constraints are imposed:

$$d_{0p} \geqslant 225, \quad d_{0z} \geqslant 0 \quad \text{and} \quad l_3 \geqslant 105 \ (mm).$$

In order to locate the third actuator away from the Z-axis as depicted in Fig. 1, we add

$$e_x \geqslant d_{0p} + \Delta d_1 + l_3 \quad \text{and} \quad e_y \geqslant 224 \ (mm).$$

Table 1 Optimized design parameters.

Design Variables	Optimum Values (mm)
d_{0p}	225.0
d_{0z}	226.8
e_x	914.4
e_y	223.9
l_{p1}	400.0
l_{p2}	373.0
l_{z1}	406.0
l_{z2}	384.0
l_3	105.0

Finally, to prevent the elbows of the first and second limbs from hitting a workpiece in the prescribed workspace, two additional inequality constraints are added:

$$\theta_{12} \leqslant 30^\circ \quad \text{and} \quad \theta_{22} \geqslant 60^\circ.$$

Sequential Quadratic Programming, which is known to be more efficient than the method of penalty function [34], is used as the solution technique for the constrained optimization problem. The total number of grid points used for the optimization is $41 \times 41 \times 31 = 52{,}111$. The optimized value of the global design index is $\eta = 3.2729\ \mathrm{m}^{-2}$. Table 1 shows the optimal design parameters. Figure 7 shows an assembly drawing and Fig. 8 shows a prototype machine constructed by using the optimized design parameters.

7 Conclusions

A new 3-DOF translational parallel manipulator, behaving like a conventional X-Y-Z Cartesian machine, is conceived. Two actuation methods are evaluated. The evaluation includes the forward and inverse kinematics, the Jacobian analysis, the static force analysis, and the singularity analysis. The rotary actuation method is judged to be impractical because of the existence of singularities inside its workspace. The effects of misalignment of linear actuators on the motion of the moving platform are discussed. The stiffness and workspace optimization of the manipulator is performed for the linear actuation method. Finally, a prototype CPM has been constructed to demonstrate the principle.

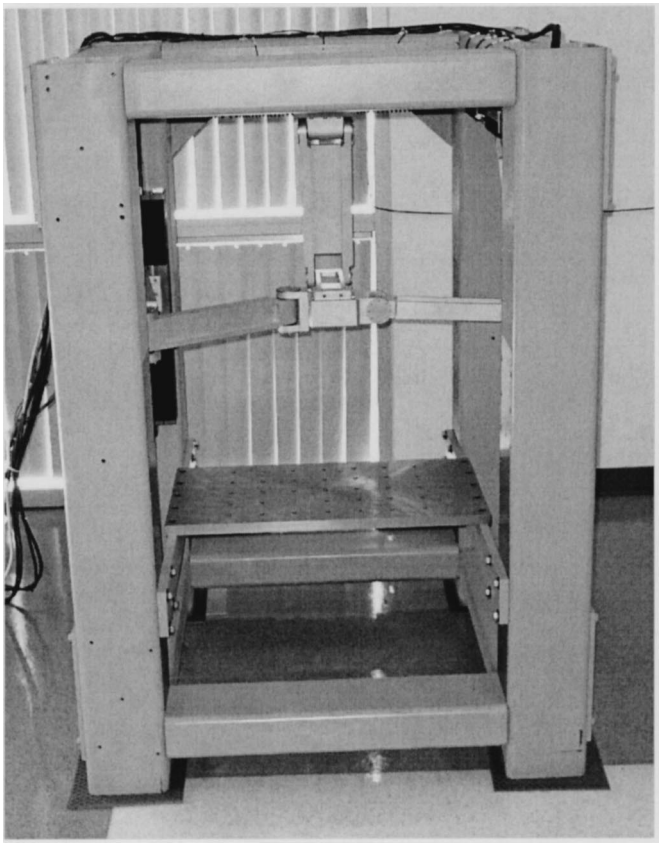

Fig. 8 Prototype Cartesian parallel manipulator

Future research will focus on the kinematic calibration and error compensation, and on improving the accuracy of the machine.

Acknowledgment

This work is supported in part by the Department of Mechanical Engineering, Bourns College of Engineering, at the University

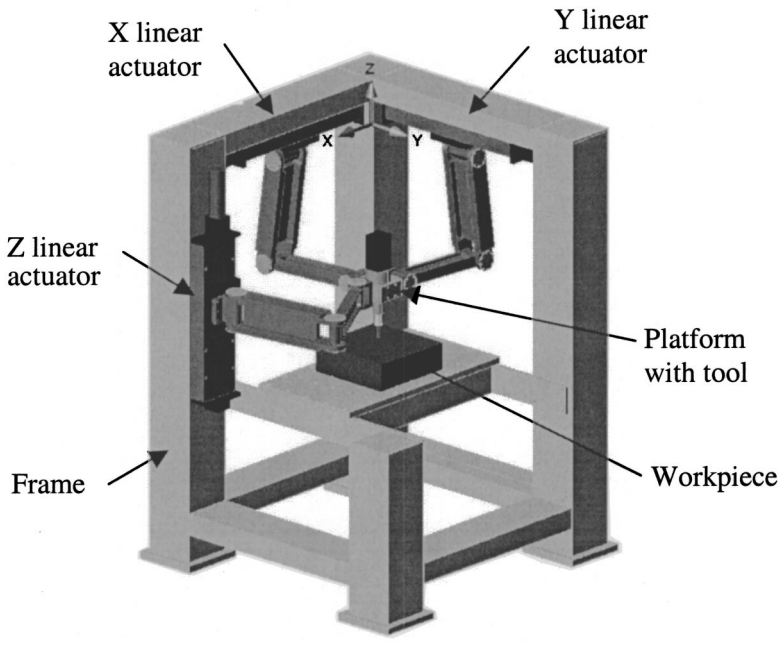

Fig. 7 Assembly drawing of a prototype parallel manipulator

of California, Riverside, and in part by postdoctoral fellowships program from Korea Science & Engineering Foundation (KOSEF).

Nomenclature

In general, a leading superscript is used to denote the coordinate system in which a vector is express. A single subscript is used to indicate the limb number or the x, y, or z component of a vector. When two subscripts are used, the first subscript generally denotes the limb number and the second subscript represents the link number of a limb or the x, y, or z component of a vector.

References

[1] Lee, K., and Shah, D. K., 1987, ''Kinematics Analysis of a Three Degrees of Freedom In-Parallel actuated Manipulator,'' *Proc. IEEE International Conf. on Robotics and Automation*, Vol. 1, pp. 345–350.

[2] Yang, P. H., Waldron, K. J., and Orin, D. E., 1996, ''Kinematics of a Three Degrees-Of-Freedom Motion Platform for a Low-Cost Driving Simulator,'' *Recent Advances in Robot Kinematics*, J. Lenarcic and V. Parenti-Castelli, eds., Kluwer Academic Publishers, London, pp. 89–98.

[3] Ceccarelli, M., 1997, ''A New 3 D.O.F. Spatial Parallel Mechanism,'' Mech. Mach. Theory, **32**(8), pp. 895–902.

[4] Gosselin, C. M., and Angeles, J., 1989, ''The Optimum Kinematic Design of a Spherical Three-Degree-of-Freedom Parallel Manipulator,'' ASME J. Mech. Autom. Des., **111**(2), pp. 202–207.

[5] Karouia, M., and Herve, J. M., 2000, ''A Three-DOF Tripod for Generating Spherical Rotation,'' *Advances in Robot Kinematics*, J. Lenarcic and V. Parenti-Castelli, eds., Kluwer Academic Publishers, pp. 395–402.

[6] Vischer, P., and Clavel, R., 2000, ''Argos: a Novel 3-DOF Parallel Wrist Mechanism,'' Int. J. Robot. Res., **19**(1), pp. 5–11.

[7] Di Gregorio, R., 2001, ''A New Parallel Wrist Using only Revolute Pairs: The 3-RUU Wrist,'' Robotica, **19**(3), pp. 305–309.

[8] Zlatanov, D., Bonev, I., and Gosselin, C. M., 2002, ''Constraint Singularities of Parallel Mechanisms,'' *Proc. of IEEE International Conference on Robotics and Automation*, Washington, D. C., pp. 496–502.

[9] Fang, Y., and Tsai, L. W., 2002, ''Structure Synthesis of 3-DOF Rotational Parallel Manipulators,'' submitted to IEEE Trans. Rob. Autom. .

[10] Clavel, R. 1988, ''Delta, a Fast Robot with Parallel Geometry,'' *18th International Symposium on Industrial Robots*, Sydney, Australia, pp. 91–100.

[11] Pierrot, F., Reynaud, C., and Fournier, A., 1990, ''DELTA: A Simple and Efficient Parallel Robot,'' Robotica, **8**, pp. 105–109.

[12] Tsai, L. W., Walsh, G. C., and Stamper, R., 1996, ''Kinematics of a Novel Three DOF Translational Platform,'' *Proc. of the 1996 IEEE International Conference on Robotics and Automation*, Minneapolis, MN, pp. 3446–3451.

[13] Tsai, L. W., 1997, ''Multi-degree-of-freedom Mechanisms for Machine Tools and the Like,'' U.S. Patent, No. 5,656,905.

[14] Tsai, L. W., 1996, ''Kinematics of a Three-DOF Platform Manipulator with Three Extensible Limbs,'' *Advances in Robot Kinematics*, J. Lenarcic and V. Parenti-Castelli, eds., Kluwer Academic Publishers, pp. 401–410.

[15] Di Gregorio, R., and Parenti-Castelli, V., 1998, ''A Translational 3-DOF Parallel Manipulator,'' *Advances in Robot Kinematics*, J. Lenarcic and M. L. Husty, eds., Kluwer Academic Publishers, London, pp. 49–58.

[16] Tsai, L. W., and Joshi, S., 2000, ''Kinematics and Optimization of a Spatial 3-UPU Parallel Manipulator,'' ASME J. Mech. Des., **122**(4), pp. 439–446.

[17] Tsai, L. W., and Joshi, S., 2002, ''Kinematic Analysis of 3-DOF Position Mechanism for Use in Hybrid Kinematic Machines,'' ASME J. Mech. Des., **124**(2), pp. 245–253.

[18] Herve, J. M., and Sparacino, F., 1991, ''Structural Synthesis of Parallel Robots Generating Spatial Translation,'' *5th IEEE International Conference on Advanced Robotics*, Pisa, Italy, pp. 808–813.

[19] Zhao, T. S., and Huang, Z., 2000, ''A Novel Three-DOF Translational Platform Mechanism and Its Kinematics,'' *Proc. of the 2000 ASME Design Engineering Technical Conferences*, Baltimore, MD, MECH-14101.

[20] Wenger, P., and Chablat, D., 2000, ''Kinematic Analysis of a New Parallel Machine Tool: The Orthoglide,'' *Advances in Robot Kinematics*, J. Lenarcic and M. L. Stanisic, eds., Kluwer Academic Publishers, London, pp. 305–314.

[21] Baron, L., and Bernier, G., 2001, ''The Design of Parallel Manipulators of Star Topology Under Isotropic Constraint,'' *Proc. of the 2001 ASME Design Engineering Technical Conferences*, Pittsburgh, PA, DAC-21025.

[22] Baron, L., G., 2001, ''Workspace-based Design of Parallel Manipulators of Star Topology with a Genetic Algorithm,'' *Proc. of the 2001 ASME Design Engineering Technical Conferences*, Pittsburgh, PA, DAC-21026.

[23] Herve, J. M., 1992, ''Star, a New Concept in Robotics,'' *3rd International Workshop on Advances in Robotics Kinematics*, Ferrara, Italy, pp. 176–183.

[24] Carricato, M., and Parenti-Castelli, V., 2001, ''A Family of 3-DOF Translational Parallel Manipulators,'' *Proc. of the 2001 ASME Design Engineering Technical Conferences*, Pittsburgh, PA, DAC-21035.

[25] Carricato, M., and Parenti-Castelli, V., 2001, ''Position Analysis of a New Family of 3-DOF Translational Parallel Manipulators,'' *Proc. of the 2001 ASME Design Engineering Technical Conferences*, Pittsburgh, PA, DAC-21036.

[26] Kong, X., and Gosselin, C. M., 2002, ''Type Synthesis of Linear Translational Parallel Manipulators,'' *Advances in Robot Kinematics*, J. Lenarcic and V. Parenti-Castelli, eds., Kluwer Academic Publishers, pp. 453–462.

[27] Kong, X., and Gosselin, C., 2001, ''Generation of Parallel Manipulators with Three Translational Degrees of Freedom Based on Screw Theory,'' *Proceedings of IFToMM Symposium on Mechanisms, Machines, and Mechatronics*, Saint-Hubert, Canada.

[28] Fang, Y., and Tsai, L. W., 2002, ''Enumeration of 3-DOF Translational Parallel Manipulators Using the Theory of Reciprocal Screws,'' accepted for publication in ASME J. Mech. Des., .

[29] Carricato, M., and Parenti-Castelli, V., 2002, ''Singularity-Free Fully-Isotropic Translational Parallel Manipulators,'' *2002 ASME International Design Engineering Technical Conferences*, Sep. 29-Oct. 2, 2002, Montreal, Canada, DETC2002/MECH-34323.

[30] Carricato, M., and Parenti-Castelli, V., 2002, ''Comparative Position, Workspace and Singularity Analyses of Two Isotropic Translational Parallel Manipulators with Three 4-DOF Legs,'' *Proc. of MUSMe 2002, International Symposium on Multibody Systems and Mechatronics*, Mexico City, Mexico, Paper No. M22.

[31] Kong, X., and Gosselin, C. M., 2002, ''Kinematics and Singularity Analysis of 3-CRR 3-DOF Translational Parallel Manipulators,'' Int. J. Robot. Res., *in press*.

[32] Tsai, L. W., 1999, *Robot Analysis: The Mechanics of Serial and Parallel Manipulators*, John Wiley & Sons, pp. 224–226.

[33] Stamper, R. E., Tsai, L. W., and Walsh, G. C., 1997, ''Optimization of a Three DOF Translational Platform for Well-Conditioned Workspace,'' *Proc. 1997 IEEE International Conf. on Robotics and Automation*, Albuquerque, NM, paper No. A1-MF-0025.

[34] Fletcher, R., 1980, ''Practical Methods of Optimization,'' Vol. 2, *Constrained Optimization*, John Wiley and Sons.